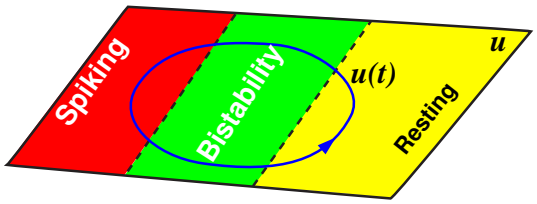

Figure 9.11: Parameter u can control spiking behavior of the fast subsystem in (9.1). When u changes slowly, the model exhibits bursting behavior.

synaptic by Skinner et al. (1994):

- INTRINSIC RELEASE: The active cell stops spiking, terminates inhibition and allows inhibited cell to fire.
- INTRINSIC ESCAPE: Inhibited cell recovers, starts to fire and shuts off the active cell.
- SYNAPTIC RELEASE: The inhibition weakens, e.g., due to spike frequency adaptation or short-term synaptic depression, and allows the inhibited cell to fire.
- SYNAPTIC ESCAPE: Inhibited cell depolarizes above certain threshold and starts to inhibit the active cell.

All four mechanisms assume that in addition to fast variables responsible for spiking, there are also slow adaptation variables responsible for slowing down or termination of spiking, recovery, or synaptic depression. Thus, similarly to the minimal models above, the circuit has at least two time scales, i.e., it is a fast-slow system.

9.2 Geometry

To understand the neuro-computational properties of bursters, we need to study the geometry of their phase portraits. In general, it is quite a difficult task. However, it can be accomplished in the special case of fast-slow dynamics.

9.2.1 Fast-slow bursters

We say that a neuron is a *fast-slow burster* if its behavior can be described by a fast-slow system of the form

$$\begin{array}{rcll} \dot{x} & = & f(x,u) & \text{(fast spiking)} \\ \dot{u} & = & \mu g(x,u) & \text{(slow modulation)} \end{array} \tag{9.1}$$

Vector $x \in \mathbb{R}^m$ describes fast variables responsible for spiking. It includes the membrane potential V, activation and inactivation gating variables for fast currents, etc. Vector $u \in \mathbb{R}^k$ describes relatively slow variables that modulate fast spiking, e.g., gating variable of a slow K^+current, intracellular concentration of Ca^{2+} ions, etc. Small parameter μ represents the ratio of time scales between spiking and modulation. When

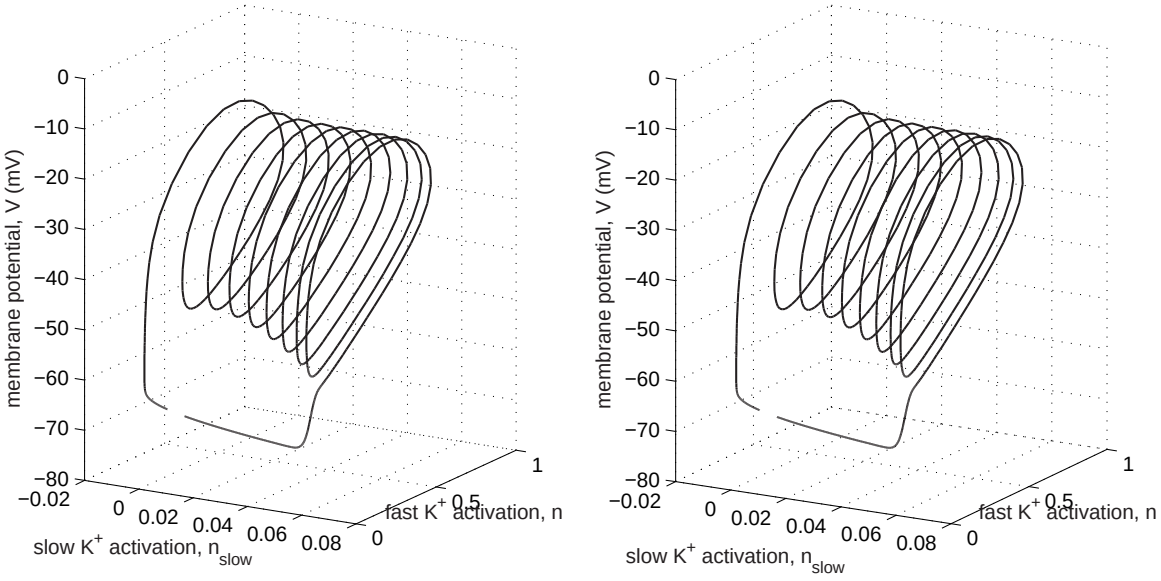

Figure 9.12: Stereoscopic image of a bursting trajectory of the $I_{\mathrm{Na,p}}$+I_{K}+$I_{\mathrm{K(M)}}$-model in the three-dimensional phase space $(V, n, n_{\mathrm{slow}})$ (for cross-eye viewing).

we analyze models, we assume that $\mu \ll 1$; that is, it could be as small as we wish. The results obtained via such an analysis may not have any sense when μ is of the order 0.1 or greater.

To analyze bursters, we first assume that $\mu = 0$, so that we can consider the fast and slow systems separately. This constitutes the method of *dissection* of neural bursting pioneered by Rinzel (1985). In fact, we have done this many times in the previous chapters when we substituted $m = m_\infty(V)$ into the voltage equation. The fast subsystem can be resting (but excitable), bistable, or spiking depending on the value of u; see Fig. 9.11. Bursting occurs when u visits the spiking and quiescent areas periodically. Many important aspects of bursting behavior can be understood via phase portrait analysis of the fast subsystem

$$\dot{x} = f(x, u)\ , \qquad x \in \mathbb{R}^m\ ,$$

treating $u \in \mathbb{R}^k$ as a vector of slowly changing bifurcation parameters.

We say that the burster is of the "m+k" type when the fast subsystem is m-dimensional and the slow subsystem is k-dimensional. There are some "1+1" and "2+0" bursters, see Ex.1 – Ex.4, though they do not correspond to any known neuron. Most of the bursting models in this chapter are of the "2+1" and "2+2" type.

9.2.2 Phase portraits

Since most bursting models are at least of the "2+1" type, their phase space is at least three-dimensional. Analyzing and depicting multi-dimensional phase portraits is

challenging. Even understanding the geometry of a single bursting trajectory depicted in Fig. 9.12 is difficult unless one uses a stereoscope.

In Fig. 9.13 we investigate geometrically the $I_{\mathrm{Na,p}}+I_{\mathrm{K}}+I_{\mathrm{K(M)}}$-model, which is a fast-slow burster of the "2+1" type. The naked bursting trajectory is depicted in the lower left corner. We set $\mu = 0$ (i.e., $\tau_{\mathrm{slow}}(V) = +\infty$) and slice the three-dimensional space by planes n_{slow} =const, depicted in the top right corner. Phase portraits of the two-dimensional fast subsystem with fixed n_{slow} are depicted in the middle of the figure. Notice how the limit cycle attractors and the equilibria of the fast subsystem depend on the value of n_{slow}. Gluing the phase portraits together, we see that there is a manifold of limit cycle attractors (shaded cylinder) that starts when $n_{\mathrm{slow}} < 0$ and ends at the saddle homoclinic orbit bifurcation when $n_{\mathrm{slow}} = 0.066$. There is also a locus of stable and unstable equilibria that appears via a saddle-node bifurcation when $n_{\mathrm{slow}} = 0.0033$.

Once we understand the transitions from one phase portrait to another as the slow variable changes, we can understand the geometry of the burster. Suppose $\mu > 0$ (i.e., $\tau_{\mathrm{slow}}(V) = 20$ ms) so that n_{slow} can evolve according to its gating equation.

Let us start with the membrane potential at the stable equilibrium corresponding to resting state. The parameters of the $I_{\mathrm{Na,p}}+I_{\mathrm{K}}+I_{\mathrm{K(M)}}$-model (see caption to Fig. 9.4) are such that slow K^+ M-current deactivates at rest, i.e., n_{slow} slowly decreases, and the bursting trajectory slides along the bold half-parabola corresponding to the locus of stable equilibria. After a while, the K^+ becomes so small, that it cannot hold the membrane potential at rest. This happens when n_{slow} passes the value 0.0033, the stable equilibrium coalesces with an unstable equilibrium (saddle), and they annihilate each other via saddle-node bifurcation. Since the resting state no longer exists (see phase portrait at the top left of Fig. 9.13) the trajectory jumps up to the stable limit cycle corresponding to repetitive spiking. This jumping corresponds to the transition from resting to spiking behavior.

While the fast subsystem fires spikes, the K^+ M-current slowly activates, i.e., n_{slow} slowly increases. The bursting trajectory winds up around the cylinder corresponding to the manifold of limit cycles. Each rotation corresponds to firing a spike. After the 9th spike in the figure, the K^+ current becomes so large that repetitive spiking cannot be sustained. This happens when n_{slow} passes the value 0.066, the limit cycle becomes a homoclinic orbit to a saddle, and then disappears. The bursting trajectory jumps down to the stable equilibrium corresponding to the resting state. This jumping corresponds to the termination of active phase of bursting and transition to resting. While at rest, K^+ current deactivates, n_{slow} decreases, and so on.

Figure 9.13 presents the guts of the geometrical mechanism of bursting of the $I_{\mathrm{Na,p}}+I_{\mathrm{K}}+I_{\mathrm{K(M)}}$-model with parameters as in Fig. 9.4. Other values of the parameters can result in different geometrical mechanisms, summarized in Sect. 9.3. In all cases, our approach is the same: freeze the slow subsystem by setting $\mu = 0$; analyze phase portraits of the fast subsystem treating the slow variable as a bifurcation parameter; then glue the phase portraits, let $\mu \neq 0$ but small, and see how the evolution of the slow subsystem switches the fast subsystem between spiking and resting states.

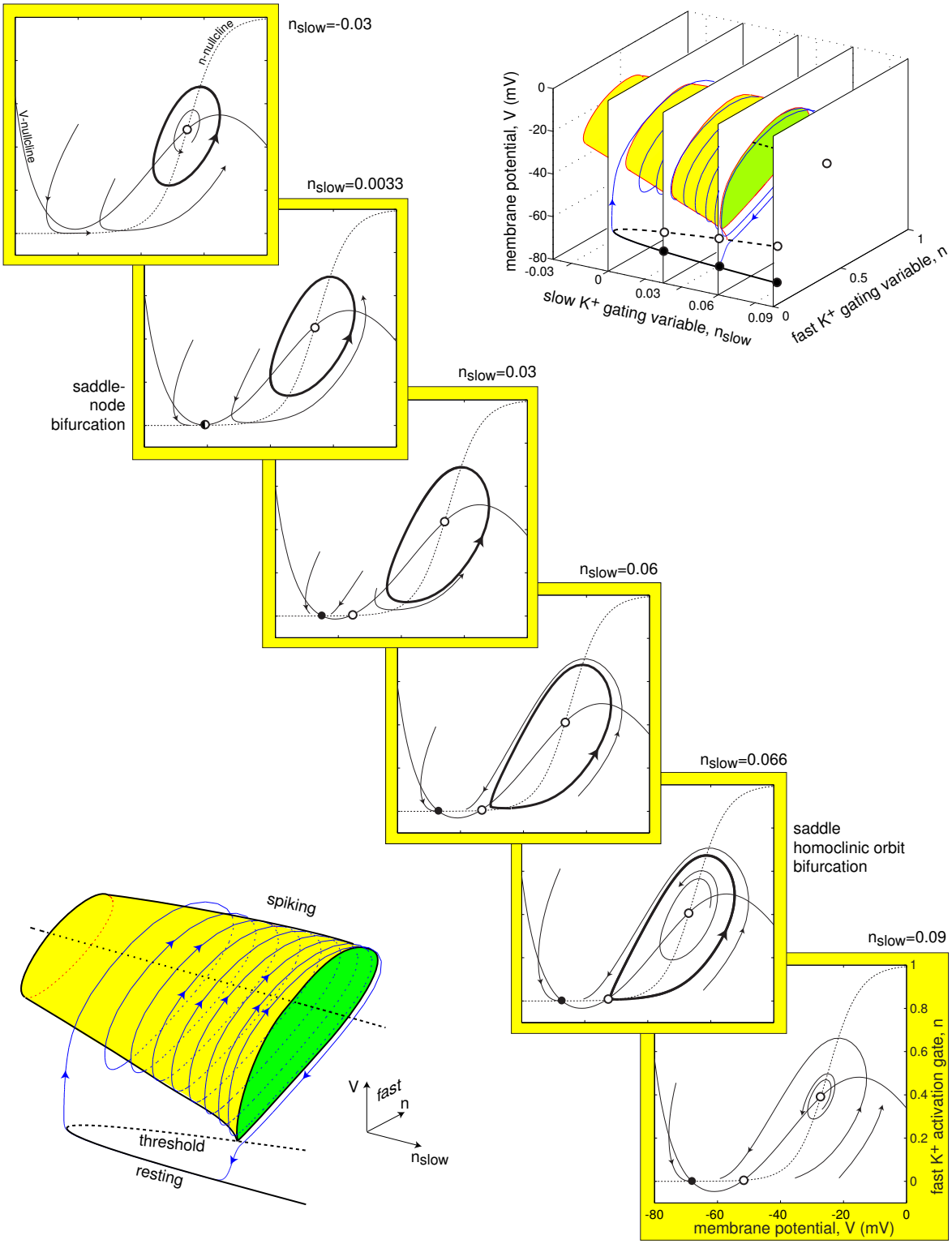

Figure 9.13: Bursting trajectory of the $I_{\mathrm{Na,p}}$+I_{K}+$I_{\mathrm{K(M)}}$-model in three-dimensional phase space and its slices n_{slow} = const.

The method usually breaks down if μ is not small enough, because evolution of the "slow" variable starts to interfere with that of the fast variable. How small is *small* depends on the particulars of the equations describing bursting activity. One should worry when μ is greater than 0.1.

9.2.3 Averaging

What governs the evolution of the slow variable u? To study this question, we describe a well-known and widely used method that reduces the fast-slow system (9.1) to its slow component. In fact, we have already used this method in Chap. 3 and 4 to reduce the dimension of neuronal models via substitution $m = m_\infty(V)$. Using essentially the same ideas, we take advantage of the two time scales in (9.1) and get rid of the fast subsystem via substitution $x = x(u)$.

When the neuron is resting, its membrane potential is at an equilibrium and all fast gating variables are at their steady-state values, so that $x = x_{\rm rest}(u)$. Using this function in the slow equation in (9.1) we obtain

$$\dot{u} = \mu g(x_{\rm rest}(u), u) \qquad \text{(reduced slow subsystem)}\ , \tag{9.2}$$

which can easily be studied using the geometrical methods presented in Chap. 3 or 4.

Let us illustrate all the steps involved using the $I_{\rm Na,p}$+$I_{\rm K}$+$I_{\rm K(M)}$-model with $n_{\rm slow}$ being the gating variable of the slow K^+ M-current. First, we freeze the slow subsystem, i.e., set $\tau_{\rm slow}(V) = \infty$ so that $\mu = 1/\tau_{\rm slow} = 0$, and determine numerically the resting potential $V_{\rm rest}$ as a function of the slow variable $n_{\rm slow}$. The function $V = V_{\rm rest}(n_{\rm slow})$ is depicted in Fig. 9.14, top, and it coincides with the solid half-parabola in Fig. 9.13. Then, we use this function in the gating equation for the M-current to obtain (9.2)

$$\dot{n}_{\rm slow} = (n_{\infty,\rm slow}(V_{\rm rest}(n_{\rm slow})) - n_{\rm slow})/\tau_{\rm slow}(V_{\rm rest}(n_{\rm slow})) \quad = \bar{g}(n_{\rm slow})$$

depicted in Fig. 9.14, bottom. Notice that $\bar{g} < 0$ meaning that $n_{\rm slow}$ decreases while the fast subsystem rests. The rate of decrease is fairly small when $n_{\rm slow} \approx 0$.

A similar method of reduction, with an extra step, can be used when the fast subsystem fires spikes. Let $x(t) = x_{\rm spike}(t, u)$ be a periodic function corresponding to an infinite spike train of the fast subsystem when u is frozen. Slices of this function are depicted in Fig. 9.14, top. Let $T(u)$ be the period of spiking oscillation. The periodically forced slow subsystem

$$\dot{u} = \mu g(x_{\rm spike}(t, u), u) \qquad \text{(slow subsystem)} \tag{9.3}$$

can be averaged and reduced to a simpler model

$$\dot{w} = \mu \bar{g}(w) \qquad \text{(averaged slow subsystem)} \tag{9.4}$$

by a near-identity change of variables $w = u + o(\mu)$, where $o(\mu)$ denotes small terms of order μ or less. Here

$$\bar{g}(w) = \frac{1}{T(w)} \int_0^{T(w)} g(x_{\rm spike}(t, w), w)\, dt$$

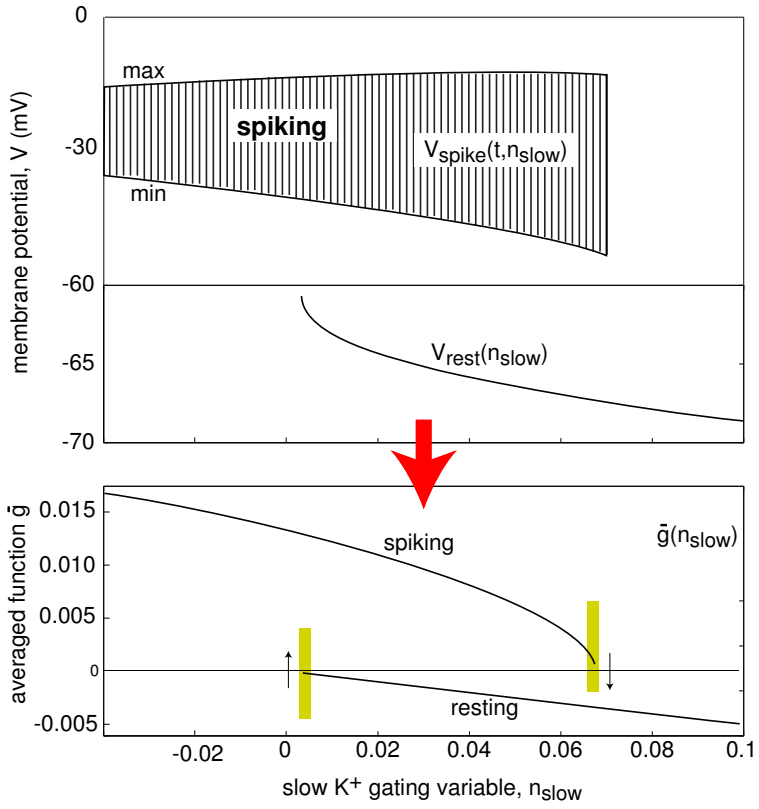

Figure 9.14: Spiking solutions $V(t) = V_{\rm spike}(t, u_{\rm slow})$, resting membrane potential $V = V_{\rm rest}(n_{\rm slow})$, and the reduced slow subsystem $\dot{n}_{\rm slow} = \bar{g}(n_{\rm slow})$ of the $I_{\rm Na,p}$+$I_{\rm K}$+$I_{\rm K(M)}$-model. The reduction is not valid in the shaded regions.

is the average of g, depicted in Fig. 9.14, bottom, for the $I_{\rm Na,p}$+$I_{\rm K}$+$I_{\rm K(M)}$-model. Check that $\bar{g}(w) = g(x_{\rm rest}(w), w)$ when the fast subsystem is resting. Limit cycles of the averaged slow subsystem corresponds to bursting dynamics, whereas equilibria correspond to either resting or periodic spiking states of the full system (9.1) – the result known as Pontryagin–Rodygin (1960) theorem. Interesting regimes correspond to the co-existence of limit cycles and equilibria of the slow averaged system.

We purposely used a different letter, w, to denote the new slow variable to stress that (9.4) is not equivalent to (9.3). Their solutions are $o(\mu)$-close to each other only when certain conditions are satisfied, see Guckenheimer and Holmes (1983) or Hoppensteadt and Izhikevich (1997). In particular, this straightforward averaging breaks down when u passes slowly the bifurcation values. For example, the period, $T(u)$, of $x_{\rm spike}(t, u)$ may go to infinity, as happens near saddle-node on invariant circle and saddle homoclinic orbit bifurcations, or transients may take as long as $1/\mu$, or the averaged system (9.4) is not smooth. All these cases are encountered in bursting models. Thus, one can use the reduced slow subsystem only when the fast subsystem is sufficiently far away from a bifurcation, e.g., away from the shaded regions in Fig. 9.14.

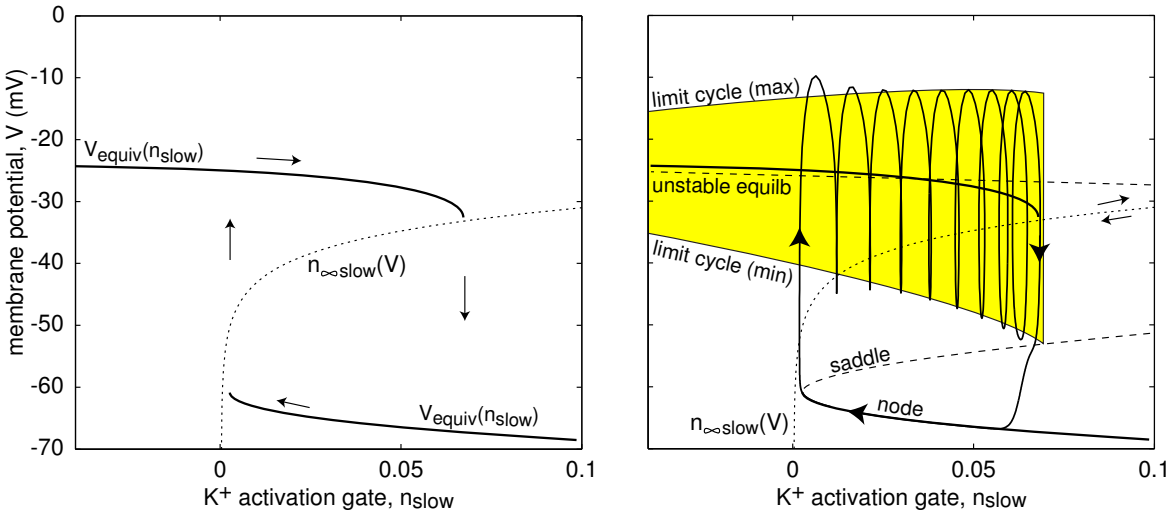

Figure 9.15: Projection of bursting trajectory of the $I_{\mathrm{Na,p}}$+I_{K}+$I_{\mathrm{K(M)}}$-model onto the (n_{slow}, V) plane.

9.2.4 Equivalent Voltage

Let us consider a "2+1" burster with a slow subsystem depending only on the slow variable and the membrane potential V, as in the $I_{\mathrm{Na,p}}$+I_{K}+$I_{\mathrm{K(M)}}$-model. The nonlinear equation

$$g(V, u) = \bar{g}(u) \tag{9.5}$$

can be solved for V. The solution, $V = V_{\mathrm{equiv}}(u)$, is referred to as being the *equivalent voltage* (Kepler et al. 1992, Bertram et al. 1995), because it substitutes the periodic function $x_{\mathrm{spike}}(t, u)$ in (9.3) by an "equivalent" value of the membrane potential, so that the reduced slow subsystem (9.3) has the same form,

$$\dot{u} = \mu g(V_{\mathrm{equiv}}(u), u) \qquad \text{(slow subsystem)} \ , \tag{9.6}$$

as in (9.1). Check that $V_{\mathrm{equiv}}(u) = V_{\mathrm{rest}}(u)$ when the fast subsystem is resting. An interesting mathematical possibility is when V_{equiv} during spiking is below V_{rest}, leading to bizarre bursters having amplifying slow currents, such as the one in Ex. 11.

We depict the equivalent voltage of the $I_{\mathrm{Na,p}}$+I_{K}+$I_{\mathrm{K(M)}}$-model in Fig. 9.15, left (variable u corresponds to n_{slow}). In the same figure, we depict the steady-state activation function $n = n_{\infty,\mathrm{slow}}(V)$ (notice the flipped coordinate system). We interpret the two curves as fast and slow nullclines of the reduced (V, n_{slow})-system. During the active (spiking) phase of bursting, the reduced system slides along the upper branch of $V_{\mathrm{equiv}}(n_{\mathrm{slow}})$ to the right. When it reaches the end of the branch, it falls down to the lower branch corresponding to resting, and slides along this branch to the left. When it reaches the left end of the lower branch, it jumps up to the upper branch, and thereby closes the hysteresis loop. Fig. 9.15, right, summarizes all the information needed to understand the transitions between resting and spiking states in this model. It depicts

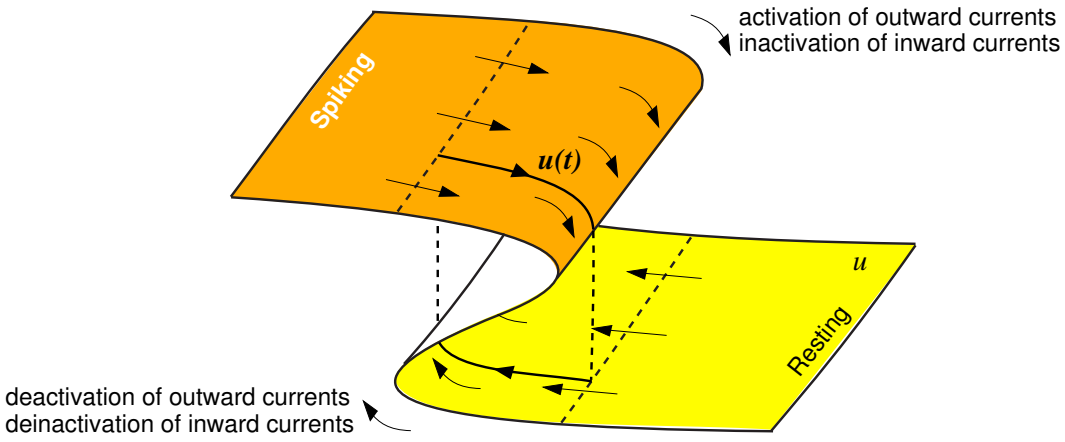

Figure 9.16: Hysteresis-loop periodic bursting.

the bursting trajectory, loci of equilibria of the fast subsystem, and voltage range of spiking limit cycle as a function of the slow gate n_{slow}. With some experience, one can read this complicated figure and visualize the three-dimensional geometry underlying bursting dynamics.

9.2.5 Hysteresis loops and slow waves

Sustained bursting activity of the fast-slow system (9.1) corresponds to periodic (or chaotic) activity of the reduced slow subsystem (9.6). Depending on the dimension of u, i.e., on the number of slow variables, there could be two fundamentally different ways the slow subsystem oscillates.

If the slow variable u is one-dimensional, then there must be a bistability of resting and spiking states of the fast subsystem so that u oscillates via a hysteresis loop. That is, the reduced equation (9.6) consists of two parts, one for $V_{\text{equiv}}(u)$ corresponding to spiking, and one for $V_{\text{equiv}}(u)$ corresponding to resting of the fast subsystem, as in Fig. 9.15, left. Such a hysteresis loop bursting can also occur when u is multi-dimensional, as we illustrate in Fig. 9.16. The vector-field on the top (spiking) leaf pushes u outside the spiking area, whereas the vector-field on the bottom (resting) leaf pushes u outside the resting area. As a result, u visits the spiking and resting areas periodically, and the model exhibits *hysteresis-loop* bursting.

If resting x does not push u into the spiking area, but leaves it in the bistable area, then the neuron exhibits *burst excitability*: It has quiescent excitable dynamics, but its response to perturbations is not a single spike, but a burst of spikes, as we illustrate in Fig. 9.17.

If the fast subsystem does not have a coexistence of resting and spiking states, then the reduced slow subsystem (9.6) must be at least two-dimensional to exhibit sustained autonomous oscillation (see though Ex. 6). Such an oscillation produces a depolarization wave that drives the fast subsystem to spiking and back, as in Fig. 9.3. We refer to such bursters as *slow-wave* bursters. Quite often, however, the slow sub-

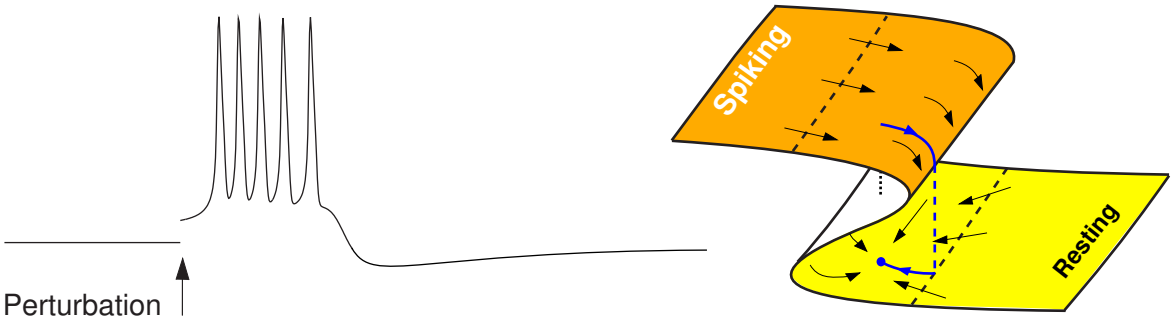

Figure 9.17: Burst excitability: A perturbation causes a burst of spikes.

system of a slow-wave burster needs the feedback from the fast subsystem to oscillate. For example, in Sect. 9.3.2 we consider slow-wave bursting of the $I_{\mathrm{Na,p}}$+I_{K}+$I_{\mathrm{Na,slow}}$ + $I_{\mathrm{K(M)}}$-model, whose slow subsystem consists of two uncoupled equations, and hence cannot oscillate by itself unless the fast subsystem is present.

9.2.6 Bifurcations "resting ↔ bursting ↔ spiking"

Switching between spiking and resting states during bursting occurs because the slow variable drives the fast subsystem through bifurcations of equilibria and limit cycle attractors. These bifurcations play an important role in our classification of bursters and in understanding their neuro-computational properties. We discuss them in detail in the next section.

Since the fast subsystem goes through bifurcations, *does this mean that the entire system (9.1) undergoes bifurcations during bursting?* The answer is NO. As long as parameters of (9.1) are fixed, the system as a whole does not undergo any bifurcations, no matter how small μ is. The system can exhibit periodic, quasi-periodic or even chaotic bursting activity, but its $m + k$-dimensional phase portrait does not change.

The only way to make system (9.1) undergo a bifurcation is to change its parameters. For example, in Fig. 9.18 we change the magnitude of the injected dc-current I in the $I_{\mathrm{Na,p}}$+I_{K}+$I_{\mathrm{K(M)}}$-model. Apparently, no bursting exists when $I = 0$. Then, repetitive bursting appears with a large interburst period that decreases as I increases. Value $I = 5$ was used to obtain bursting solutions in Fig. 9.12 and Fig. 9.13. Further increasing of I increases the duration of each burst, until it becomes infinite, i.e., bursting is transformed into tonic spiking. When $I > 8$, the slow K^+ current is not enough to stop spiking.

In Fig. 9.19 we depict the geometry of bursting in the $I_{\mathrm{Na,p}}$+I_{K}+$I_{\mathrm{K(M)}}$-model when $I = 3$, i.e., just before periodic bursting appears, and when $I = 10$, i.e., just after bursting is transformed into tonic spiking.

When $I = 3$, the nullcline of the slow subsystem $n_{\mathrm{slow}} = n_{\infty,\mathrm{slow}}(V)$ intersects the locus of stable equilibria of the fast subsystem. The intersection point is a globally stable equilibrium of the full system (9.1). Small perturbations, whether in the V direction, n direction, or n_{slow} direction subside, whereas a large perturbation, e.g., in

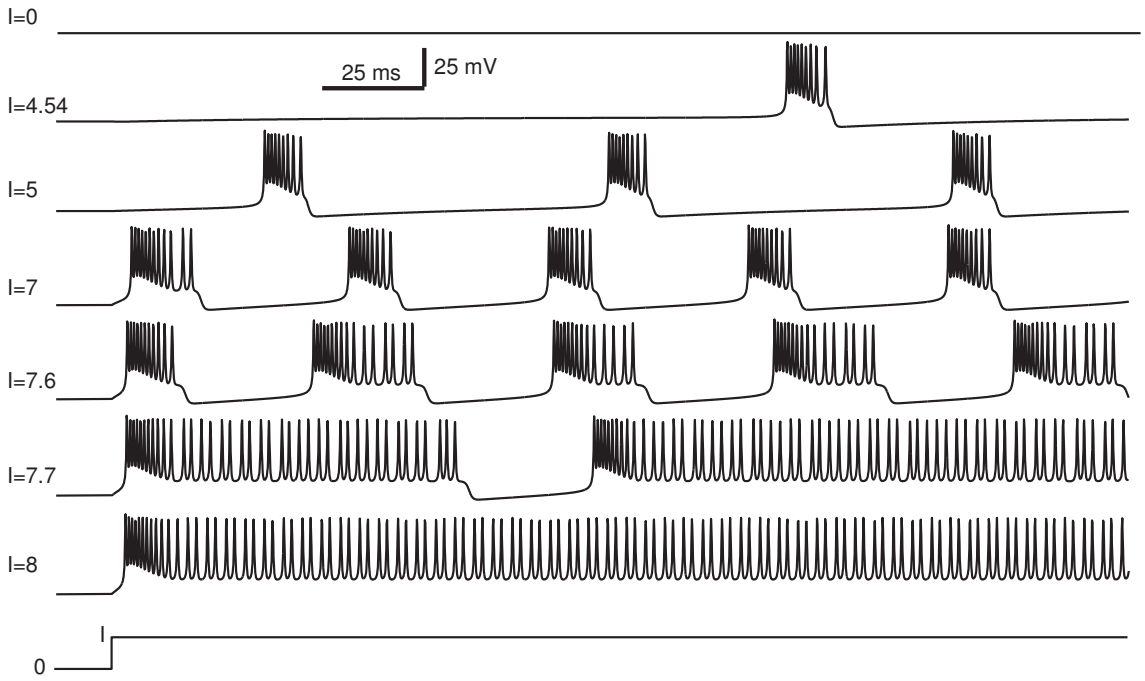

Figure 9.18: Bifurcations of bursting solutions in the $I_{\mathrm{Na,p}}$+I_{K}+$I_{\mathrm{K(M)}}$-model as the magnitude of the injected dc-current I changes.

the V direction that moves the membrane potential to the open square in the figure, initiates a transient (phasic) burst of 7 spikes. Increasing the magnitude of the injected current I shifts the saddle-node parabola to the right. When $I \approx 4.54$, the nullcline of the slow subsystem does not intersect the locus of stable equilibria, and the resting state no longer exists, as in Fig. 9.15, right. (There is still a global steady state, but it is not stable.)

Further increase of the magnitude of the injected current I results in the intersection of the nullcline of the slow subsystem with the equivalent voltage function $V_{\mathrm{equiv}}(n_{\mathrm{slow}})$. The intersection, marked by the black circle in Fig. 9.19, right, corresponds to a globally stable (spiking) limit cycle of the full system (9.1). A sufficiently strong perturbation can push the state of the fast subsystem into the attraction domain of the stable (resting) equilibrium. While the fast subsystem is resting, the slow variable decreases, i.e., K^+ current deactivates, the resting equilibrium disappears and repetitive spiking resumes.

Figures 9.18 and Fig. 9.19 illustrate possible transitions between bursting and resting, and bursting and tonic spiking. There could be other routes of emergence of bursting solutions from resting or spiking, some of them are in Fig. 9.20. Each such route corresponds to a bifurcation in the full system (9.1) with some $\mu > 0$. For example, the case $a \to 0$ corresponds to supercritical Andronov-Hopf bifurcation; the case $c \to \infty$ corresponds to a saddle-node on invariant circle or saddle homoclinic orbit bifurcation; the case $d \to \infty$ corresponds to a periodic orbit with a homoclinic structure,

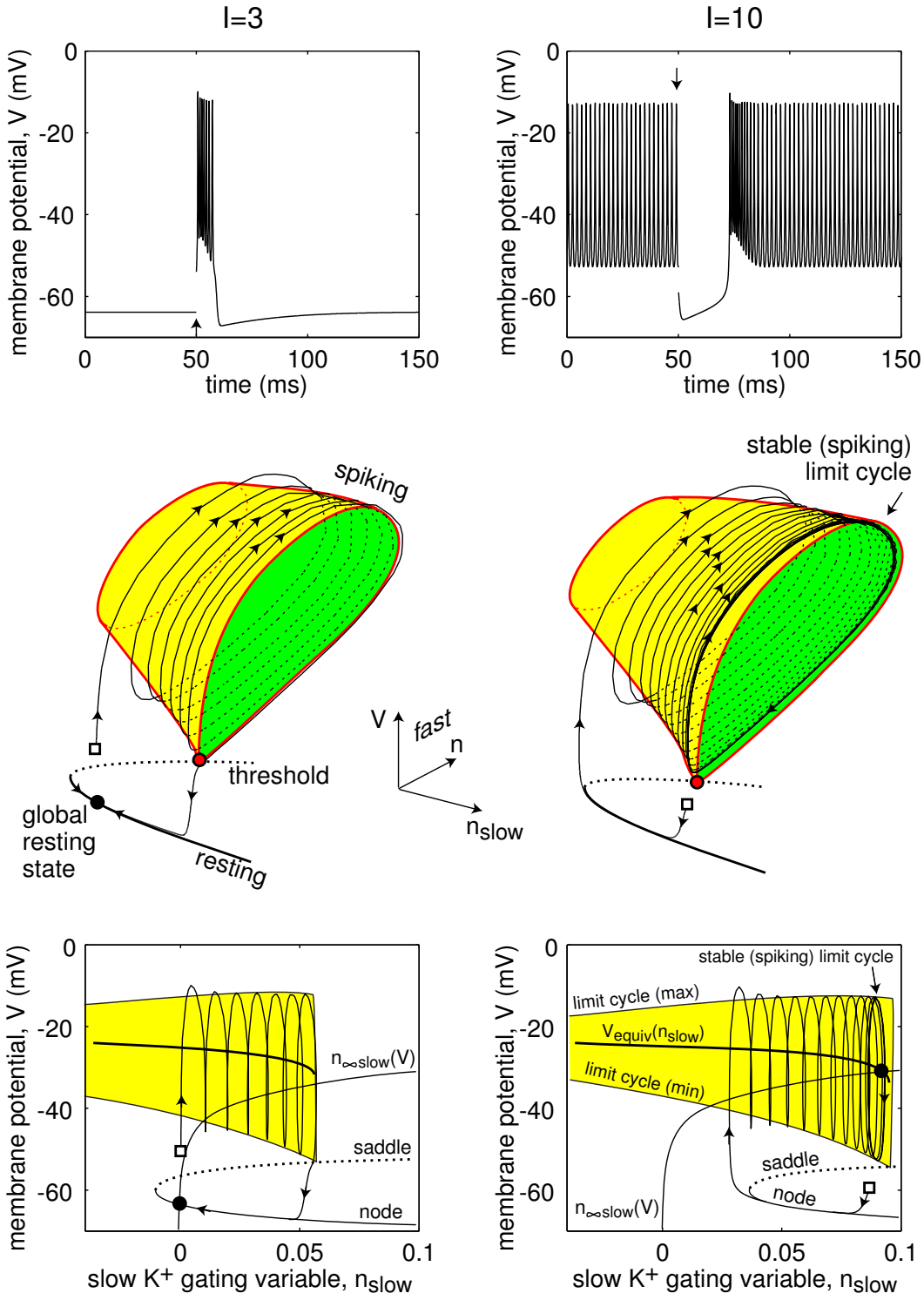

Figure 9.19: Burst excitability ($I = 3$, left) and periodic spiking ($I = 10$, right) in the $I_{\mathrm{Na,p}}$+I_{K}+$I_{\mathrm{K(M)}}$-model.

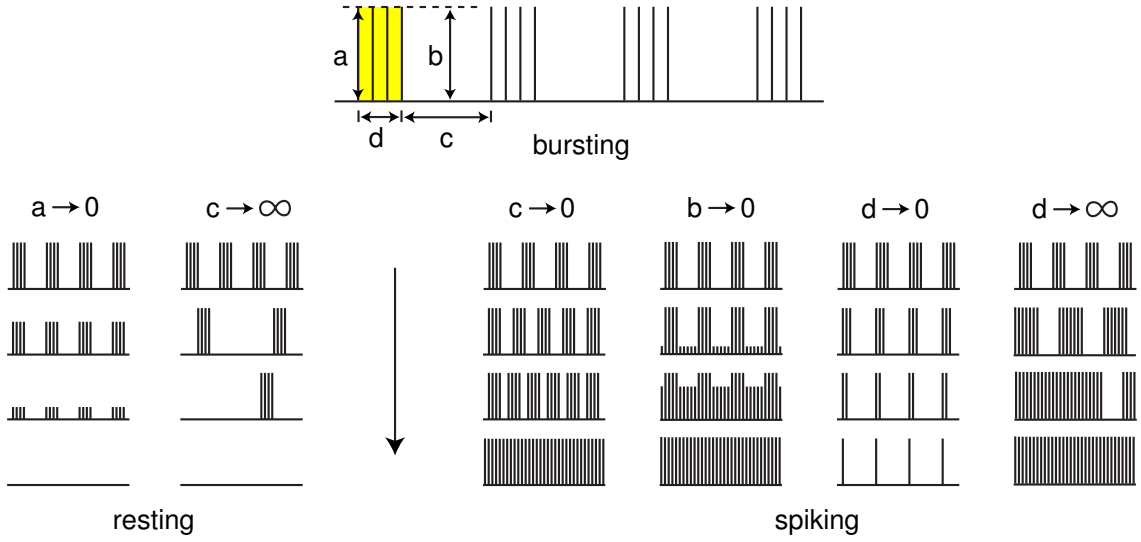

Figure 9.20: Possible transitions between repetitive bursting and resting, and repetitive bursting and repetitive spiking.

e.g., blue-sky catastrophe, fold limit cycle on homoclinic torus bifurcation, or something more complicated. The transitions "bursting ↔ spiking often exhibit chaotic (irregular) activity, so Fig. 9.20 if probably a great oversimplification. Understanding and categorizing all possible bifurcations leading to bursting dynamics is an important but open problem; see Ex. 28.

9.3 Classification

In Fig. 9.21 we identify two important bifurcations of the fast subsystem that are associated with bursting activity in the fast-slow burster (9.1):

- **(resting → spiking)** Bifurcation of an equilibrium attractor that results in transition from resting to repetitive spiking.
- **(spiking → resting)** Bifurcation of the limit cycle attractor that results in transition from spiking to resting.

These bifurcations, and not the ionic mechanisms, determine the neuro-computational properties of fast-slow bursters, discussed in Sect. 9.4. Of course, the ionic basis of bursting, i.e., the fine electrophysiological details, determine the kind of bifurcations in Fig. 9.21.

Complete topological classification of bursters based on these two bifurcations is provided by Izhikevich (2000), who identified 120 different topological types. Here, we consider only 16 planar point-cycle co-dimension-1 fast-slow bursters. We say that a fast-slow burster is *planar* when its fast subsystem is two-dimensional. We emphasize planar bursters because they have a greater chance to be encountered in computer